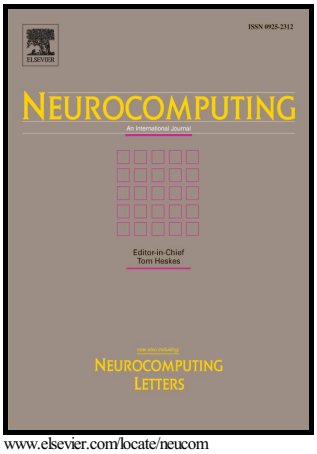

www.elsevier.com/locate/neucom

Robust Tracking and Vibration Suppression for Nonlinear Two-Inertia System via Modified Dynamic Surface Control with Error Constraint

Shubo Wang, Xuemei Ren, Jing Na, Xuehui Gao

PII: S0925-2312(16)30224-7
DOI: http://dx.doi.org/10.1016/j.neucom.2016.03.040
Reference: NEUCOM16931

To appear in: *Neurocomputing*

Received date: 27 January 2015
Revised date: 28 January 2016
Accepted date: 21 March 2016

Cite this article as: Shubo Wang, Xuemei Ren, Jing Na and Xuehui Gao, Robus Tracking and Vibration Suppression for Nonlinear Two-Inertia System via Modified Dynamic Surface Control with Error Constraint, *Neurocomputing* http://dx.doi.org/10.1016/j.neucom.2016.03.040

Robust Tracking and Vibration Suppression for Nonlinear Two-Inertia System via Modified Dynamic Surface Control with Error Constraint

Shubo Wang[a], Xuemei Ren[a,*], Jing Na[b], Xuehui Gao[a]

[a] *School of Automation, Beijing Institute of Technology, Beijing 100081,China*
[b] *Faculty of Mechanical and Electrical Engineering, Kunming University of Science and Technology, Kunming Yunnan 650500, China*

Abstract

This paper proposes a modified dynamic surface control (DSC) for speed tracking and torsional vibration suppression for two-inertia systems with nonlinear friction. The proposed controller contains two parts: tracking controller and friction compensator. The tracking controller is designed by modifying dynamic surface control, which replaces the traditional first-order filter with a high-gain tracking differentiator (HGTD). Meanwhile, an improved prescribed performance function with error constraint is also presented and incorporated into DSC design. As for the friction compensator, the nonlinear nonsmooth friction is parameterized and then compensated using echo state neural networks (ESNs). The state observer with friction compensation is used to estimate unmeasurable load speed and torsional torque. The effectiveness of proposed control scheme is verified by simulation and experiment results.

Keywords: `Dynamic surface control, friction compensation, two-inertia system, vibration suppression, prescribed performance constraint.`

*Corresponding author.
Email addresses: `wangshubo1130@126.com` (Shubo Wang), `xmren@bit.edu.cn` (Xuemei Ren), `najing25@163.com` (Jing Na), `xhgao@163.com` (Xuehui Gao)

1. Introduction

Electric actuators are widely used for the drive systems in various industrial applications, such as servo drive, robot-arm, crane system and automotive industry. The drive system is composed of a motor connected to a load through a stiffness shaft and flexible coupling, which can be modeled as a two-inertia system. This configuration may cause the torsional vibration and lead to the failure of the drive system in some cases. In order to achieve stable operation and reduce the speed vibration, it is necessary to eliminate the torsional vibration.

In order to achieve stable operation and reduce the speed vibration, many control algorithms have been proposed to damp the torsional vibration. Among them, a Proportional-Integral-Derivative (PID) control [1, 2] is used for the speed control of a two-inertia system. Although this PID algorithm designed by using motor speed feedback is widely used in industry applications, it may cause decreased dynamic performance of drive system and may not be able to effectively suppress oscillations. To achieve highly precise control performance for a drive system, advanced control structures based on state feedbacks from state variables, such as motor speed, shaft torque, load speed and disturbance torque, are proposed in [3]. However, the state variables may not be used directly because these variables are difficult to measure in reality. Thus, the estimation and observation are needed to estimate these variables [4, 5, 6, 7, 8, 9]. In many papers, Luenberger observers are applied to observe the unmeasured state variables for the linear system with small measurement noise and nonchangeable parameter [10]. However, the performance of Luenberger observer may be unsatisfactory due to the nonlinearity, measurement noise and uncertainty. In [7], the Kalman filter is proposed for a two-inertia system. It is utilized to estimate the shaft torque, load speed and load torque of the two-inertia system. A sliding-mode and optimized PID controller with a grey estimator is proposed, where the gray estimator is used to estimate torsional torque and load speed [11].

Furthermore, artificial intelligent techniques are also utilized to suppress torsional vibration of the two-inertia system [12, 13, 14, 15, 16, 17]. A torsional vibration control approach is presented in [12], which is based on the additional feedback from the torsional torque and the load-side speed estimated by a neural network estimator. To estimate the motor-side speed for suppressing the torsional vibration, the neuro-fuzzy system is employed [13]. In [14], an adaptive sliding-mode neuro-fuzzy speed controller based on model reference adaptive structure is used to suppress torsional vibration. The modified fuzzy Luenberger observer based on the difference between the electromagnetic and estimated shaft torque [15] is reported.

The nonlinear nonsmooth friction should also be taken into account in the two-inertia system. To handle unknown nonlinearities, Recurrent Neural Networks (RNNs) and Fuzzy Logic systems (FLS) have been applied to approximate unknown nonlinearities owing to their nonlinear approximation and learning abilities [18, 19, 20, 21, 22, 23]. Recently, an echo state networks (ESNs) is reported as a simplified RNNs in [24, 25, 26]. ESNs has the function approximation capability of RNNs, but requires simpler training than RNNs. Compared with RNNs, the ESNs can easily be trained without adjusting the weights between the input layer and the hidden layer, and the connection weights of the reservoir network are not altered during the training phase. However, it is noted that the transient convergence of aforementioned classical adaptive control schemes cannot be guaranteed (e.g., the overshoot, convergence rate cannot be quantitatively studied).

Recently, a new prescribed performance control (PPC) approach is proposed [27, 28, 29, 30], to guarantee the convergence of output error to a predefined arbitrarily small region, where the convergence rate should be no less than a prespecified value. In [31], an improved prescribed performance function is proposed and incorporated into the controller design for the turntable servo system. An adaptive control with prescribed performance function is proposed for suspension systems to guarantee the error convergence rate, maximum overshoot and steady-state error within a predefined region [32]. However, to our best

knowledge, the prescribed performance control has not yet been applied for the nonlinear two-inertia system.

In this paper, we propose a recursive feedback controller for the nonlinear two-inertia system with PPC. Inspired by [30], an improved prescribed performance function with error constraint is proposed and incorporated into the controller design. A recursive feedback controller is designed by modifying DSC technique from all state variables. In particular, the nonlinear friction of the two-inertia system is difficult to observe and compensate. A nonsmooth friction physics-model proposed in [33] is re-parameterized, which can capture the various friction dynamic effects such as Coulomb friction, Viscous friction, Static friction and Stribeck effect. Then, the unknown nonlinear nonsmooth friction force is approximated by ESNs, and compensated online. In order to obtain the state variables, the state observer with the estimated friction is employed to estimate the unmeasured load speed and torsional torque. Simulations and experiments based on a realistic test rig are utilized to validate the proposed control scheme. The main contributions of this paper can be summarized as follows.

1. An improved prescribed performance function is developed and incorporated into the control design of DSC for the nonlinear two-inertia system, and the tracking error is ensured within a prescribed region.

2. A new dynamic surface controller is designed by using the high-gain tracking differentiator (HGTD) to replace the first-order filter in virtual intermediate control signal. The use of HGTD can lead to better transient performance than first-order filter in the classical DSC.

3. The nonlinear nonsmooth friction model has been further parameterized, and then ESNs are used to successfully online approximate and compensate for these nonlinear nonsmooth dynamics.

4. The state observer with estimation of friction is designed to observe unmeasured load speed and torsional torque.

The rest of this paper is organized as follows. Section 2 provides a description of the nonlinear two-inertia system, the structure of ESNs, and an improved

prescribed performance function. Section 3 designs a speed control by using the modified DSC and friction compensation. The stability of closed-loop system is given in Section 4. Section 5 presents simulation results. Section 6 is devoted to validate the proposed control scheme by experiments. Some conclusions are given in Section 7.

2. Problem Formulation

2.1. Mathematical Model of Nonlinear Two-Inertia System

A typical two-inertia system is composed of a servo motor connected to a load through a stiffness shaft and flexible coupling (Figure 1). The considered system could be described by the following state equation:

$$\begin{aligned}\frac{d}{dt}\begin{pmatrix}\omega_l\\ m_s\\ \omega_m\end{pmatrix} &= \begin{pmatrix}\frac{-b_f}{J_l} & \frac{1}{J_l} & \frac{b_f}{J_m}\\ -k_f & 0 & k_f\\ \frac{b_f}{J_m} & \frac{1}{J_m} & \frac{-b_f}{J_m}\end{pmatrix}\begin{pmatrix}\omega_l\\ m_s\\ \omega_m\end{pmatrix} + \begin{pmatrix}0\\ 0\\ \frac{1}{J_m}\end{pmatrix}u \\ &\quad - \begin{pmatrix}\frac{f_l}{J_l}\\ 0\\ \frac{f_m}{J_m}\end{pmatrix} - \begin{pmatrix}\frac{\tau_l}{J_l}\\ 0\\ \frac{\tau_m}{J_m}\end{pmatrix} - \begin{pmatrix}\frac{\tilde{\Delta}_1(\omega_l)}{J_l}\\ 0\\ \frac{\tilde{\Delta}_2(\omega_m)}{J_m}\end{pmatrix}\end{aligned} \tag{1}$$

where ω_m and ω_l are the motor speed and load speed, J_m and J_l are the inertia of the motor and the load, f_m and f_l represent the nonlinear friction forces at the motor side and the load side, respectively. u is the motor electromagnetic torque, m_s is the shaft torque, k_f is the torsional stiffness coefficient, b_f is damping coefficient. τ_m and τ_l are the external disturbances of the motor side and the load side, $\tilde{\Delta}_1(\omega_l)$ and $\tilde{\Delta}_2(\omega_m)$ denote the parameters uncertainties.

Assumption 1: The reference input x_d, $\dot{x}_d$, and $\ddot{x}_d$, are continuous and bounded, that is, there exists a known compact set $\Omega_0 = \{x_d, \dot{x}_d, \ddot{x}_d : x_d^2 + \dot{x}_d^2 + \ddot{x}_d^2 \leq \delta\}$, where δ is a positive constant.

Assumption 2: The disturbances τ_m, τ_l and parameters uncertainties $\tilde{\Delta}_1(\omega_l)$ and $\tilde{\Delta}_2(\omega_m)$ are bounded.

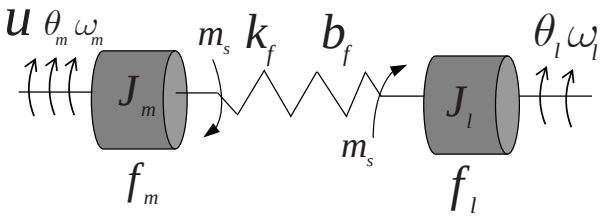

Figure 1: Two-inertia system model (θ_m and θ_l are the motor position and the load position)

.

The control objective is to design a feedback control strategy which ensures: (i) the tracking error S converges to the prescribed performance boundary; (ii) vibration in the elastic shaft is damped; (iii) the friction is compensated; (iv) all signals in the closed-loop system are bounded.

2.2. Friction Model Structure

From Figure 1, the two-inertia system mainly includes two friction forces: the motor side friction f_m and the load side friction f_l. Note that, the motor side friction force f_m is a function of the motor side velocity ω_m, while the load side friction f_l is a function of the load side velocity ω_l.

The combination of two-inertia system model (1) gives

$$J_m\dot{\omega}_m + J_l\dot{\omega}_l = u - f - d \tag{2}$$

where $f = f_m + f_l$ defines the friction force of the two-inertia system, and $d = \tau_l + \tau_m + \tilde{\Delta}_1(\omega_l) + \tilde{\Delta}_2(\omega_m)$ denotes the external disturbance and uncertainties. Thus, they can be lumped as $F = -J_l\dot{\omega}_l + f + d$ and then referred to the uncertain dynamics to be compensated on the motor side [34].

Equation (2) is used to show that the friction of two-inertia system can be lumped as an entire friction force. There are two reasons to model the entire friction force f as reflected on the motor side. First, it is not straightforward to compensate the friction separately on the load side. However, it is possible to compensate the effects of frictions entirely on the motor side. Second, from the

point view of the torque compensation, the friction force is usually compensated by operating the driving motor. In this paper, we will propose a compensation strategy to compensate the friction as an entire friction imposed on the motor side.

In order to define the characteristics of the friction f, a physics-based model named LuGre model (LG) was reported in [33], which is able to capture dynamic friction effects, such as the Stribeck effect, Hysteresis, Stick-lop limit cycling, and Rising static friction (Figure 2). The LG model is described by an internal friction state ζ governed by

$$\begin{aligned} f &= \sigma_0\zeta + \sigma_1\dot{\zeta} + \sigma_2\dot{\upsilon} \\ \dot{\zeta} &= \upsilon - |\upsilon|\zeta/h(\upsilon) \\ h(\upsilon) &= f_c + (f_s - f_c)e^{-(\upsilon^2/\upsilon_s^2)} \end{aligned} \tag{3}$$

where υ is the relative velocity between the two contacting surface at the motor side, that is, $\upsilon = \omega_m$, σ_0 is an equivalent stiffness, σ_1 is the microdamping coefficient of the internal state ζ, and σ_2 denotes the viscous friction coefficients, respectively. The function $h(\upsilon)$ is chosen to capture the Stribeck effect, where f_c and f_s are the levels of Coulomb friction and Static friction, respectively. υ_s is the Stribeck velocity, which is the velocity for the sliding friction attains its minimal value. Notice that the LG model has the following property.

Property 1[33]: It follows from (3) that $f_c \leq h(\upsilon) \leq f_s$, if $|\zeta(0)| \leq f_s/\sigma_0$, then $|\zeta(t)| \leq f_s/\sigma_0$ for all $t \geq 0$.

2.3. Function Approximation Using ESNs

Recently, the ESNs have been successfully used to model nonlinear dynamical systems [26] and also used as a state observer to estimate nonlinear function [35]. It divides the weights of the recurrent neural network into two parts: 1) a hidden layer (dynamical reservoir) with sparsely and randomly interconnected neurons, and 2) a memoryless output layer (readout). The structure of ESNs is shown in Figure 3, where the ESNs have K inputs, N neurons in the hidden layer, and L neurons in the output layer. The continuous-time dynamics of a

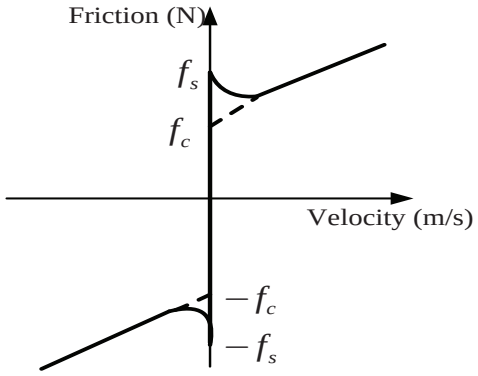

Figure 2: Basic friction of a mechanical system

leaky-integrator ESNs is given by

$$\begin{aligned} \dot{X} &= C\left(-aX + \psi(\Theta^{in}u + \Theta X + \Theta^{out}y)\right) \\ y &= G(\Theta_0^T X) \end{aligned} \tag{4}$$

where X is N-dimensional activation state, $C > 0$ is a time constant, a is the leaking decay rate, $\psi(\cdot)$ is the internal unit's activation function (sigmoids, etc.), $G(\cdot)$ is the output activation function. $\Theta^{in} \in R^{N\times K}$, $\Theta \in R^{N\times N}$, $\Theta^{out} \in R^{N\times L}$ and $\Theta_0 \in R^{L\times(K+N+L)}$ are the input weight matrix, internal weight matrix, feedback connection weights and output weight matrix, respectively.

The ESNs system performs universal approximation in the sense that for any given real continuous function $f(\cdot)$: $R^{L\times(K+N+L)} \longrightarrow R$ on a sufficiently large compact set $\Omega \subset R$ and arbitrary ε_m, ESNs system $y(x)$ exists in the form of (4) such that

$$\sup_{x\in\Omega} |f(x) - y(x)| \leq \varepsilon_m \tag{5}$$

The function $f(x)$ can be expressed as

$$f(x) = \Theta_0^{*T} X(x) + \varepsilon^* \quad \forall x \in \Omega \subset R^n \tag{6}$$

where ε^* is the error of the ESNs and $|\varepsilon^*| \leq \varepsilon_m$, the Θ_0^* is the value of Θ_0 that minimizes the approximation error ε^*. Therefore

$$\Theta_0^* = \arg \min_{\Theta_0 \in R^{L\times(K+N+L)}} \left\{ \sup_{x\in\Omega} |f(x) - \Theta_0^T X(x)| \right\} \tag{7}$$

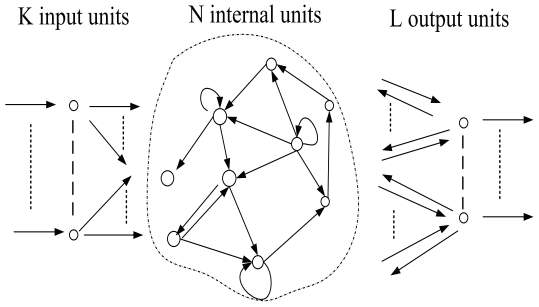

Figure 3: The basic network architecture of ESNs

Because Θ_0^* is unknown, it is replaced by the estimation value $\hat{\Theta}_0$ of Θ_0^*. Adaptive laws are required to update the parameter $\hat{\Theta}_0$ online to minimize the reference tracking error. Thus, the optimal ESNs weight can be written as

$$\hat{\Theta}_0 = \Theta_0^* + \tilde{\Theta}_0 \tag{8}$$

where $\tilde{\Theta}_0 = \hat{\Theta}_0 - \Theta_0^*$. By setting $C = 1, a = 1, G = 1$, it can be obtained from (5) that

$$X = \psi\left(\Theta^{in}u + \Theta X + \Theta^{out}y\right) \tag{9}$$

when $\dot{X} = 0$.

In this paper, we choose $X(Z) = [\varphi_1(Z), \varphi_2(Z), ..., \varphi_l(Z)]^T$ as Gaussian functions with l being the node number of ESNs output layer. That is

$$\varphi_k(Z) = \exp\left\{-\frac{(Z-\varsigma)^T(Z-\varsigma)}{\eta^2}\right\} \tag{10}$$

with $Z = [z_1, ..., z_i]^T$, $i = 1, ..., n$ being the number of input variables, ς and η are the center and radius of the Gaussian function.

2.4. Performance Function and Error Transformation

To study the transient and steady-state performances of tracking error $e(t) = [e_1(t), e_2(t), ...e_i(t)]$, a smooth decreasing function $\lambda_i(t) : \Re^+ \to \Re^+$ with $\lim_{t\to\infty} \lambda_i(t) = \lambda_{i\infty}$ will be used as prescribed performance function. In this paper, the $\lambda_i(t)$ is given as

$$\lambda_i(t) = (\lambda_{i0} - \lambda_{i\infty})e^{-c_i t} + \lambda_{i\infty} \tag{11}$$

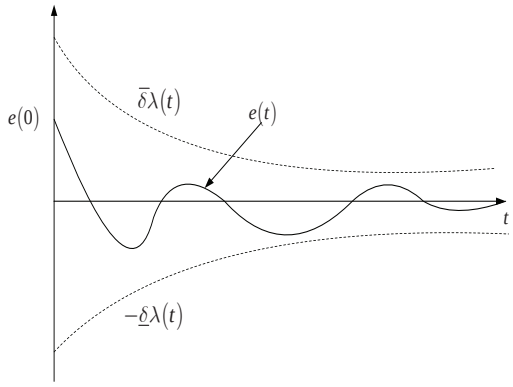

Figure 4: Basic concept of prescribed performance

where $\lambda_{i0} > \lambda_{i\infty}$ and c_i are design parameters.

According to [27], the prescribed performance is given as

$$-\underline{\delta}_i \lambda_i(t) < e_i(t) < \overline{\delta}_i \lambda_i(t), \forall t > 0 \tag{12}$$

where $-\underline{\delta}_i$ and $\overline{\delta}_i$ are design parameters.

From (11) and (12), one can see that $-\underline{\delta}_i \lambda_{i0}$ defines the lower bound of the undershoot and $\overline{\delta}_i \lambda_{i0}$ defines the upper bound of the maximum overshoot. The decreasing rate c_i denotes the required speed of convergence of the tracking errors [31]. Hence, the transient and steady-state performance can be designed a priori via tuning the parameters $-\underline{\delta}_i$, $\overline{\delta}_i$, c_i, λ_{i0}, and $\lambda_{i\infty}$. To introduce prescribed performance, an error transformation is used to transform the original nonlinear system, with the constrained tracking error behavior (12), into an equivalent "unconstrained" one. With this purpose, we define a smooth strictly increasing function $T_i(z_i)$ of transformed error z_i, which possesses the following properties:

1) $-\underline{\delta}_i < T_i(z_i) < \overline{\delta}_i$, $\forall z_i \in L\infty$.

2) $\lim_{z_i \to +\infty} T_i(z_i) = \overline{\delta}_i$, and $\lim_{z_i \to -\infty} T_i(z_i) = -\underline{\delta}_i$.

From these properties of $T_i(z_i)$, (12) is equal to

$$e_i(t) = \lambda_i(t) T_i(z_i). \tag{13}$$

Then, z_i can be written as

$$z_i = T_i^{-1}\left(\frac{e_i(t)}{\lambda_i(t)}\right). \tag{14}$$

For any initial condition $e_i(0)$, if parameters $\lambda_i(0)$, $\overline{\delta}_i$, and $\underline{\delta}_i$ are selected that $-\underline{\delta}_i\lambda_i(0) < e_i(0) < \overline{\delta}_i\lambda_i(0)$ and z_i can be controlled to be bounded, then $-\underline{\delta}_i < T_i(z_i) < \overline{\delta}_i$ holds. Then, the condition $-\underline{\delta}_i\lambda_i(t) < e_i(t) < \overline{\delta}_i\lambda_i(t)$ is guaranteed. In this paper, we propose a new prescribed transformation function combined with the virtual control of the modified DSC. A candidate transformation function is chosen as

$$T_i(z_i) = \frac{\overline{\delta}_i e^{z_i} - \underline{\delta}_i e^{-z_i}}{e^{z_i} + e^{-z_i}}. \tag{15}$$

Then, from (15), the transformed error z_i is derived as

$$z_i = T_i^{-1}\left(\frac{e_i(t)}{\lambda_i(t)}\right) = R_i\left(\frac{e_i(t)}{\lambda_i(t)}\right) = \frac{1}{2}\ln\left(\frac{e_i(t)}{\lambda_i(t)} + \underline{\delta}_i\right) - \frac{1}{2}\ln\left(\overline{\delta}_i - \frac{e_i(t)}{\lambda_i(t)}\right). \tag{16}$$

where $R_i(\cdot)$ is the inverse function of $T_i(\cdot)$. The transformed error will be utilized to ensure the prescribed output performance of the modified DSC scheme.

2.5. Luenberger State Observer

As mentioned previously, the two-inertia system is composed of a motor connected to a load machine through a shaft, which is difficult to measure all state variables. Consequently, the Luenberger state observer is designed to estimate torsional torque and the load speed. In this paper, the damping coefficient b_f is not considered because $k_f \gg b_f$.

Choose state vector $x = [\ \omega_l \quad m_s \quad \omega_m\ ]^T$, $u = m_e$, $z = -F$. Then equation (1) can be written as follows:

$$\begin{aligned} \dot{x} &= Ax + Bu + Bz \\ y &= Cx \end{aligned} \tag{17}$$

where $\mathrm{A}=\begin{pmatrix} 0 & \frac{1}{J_l} & 0 \\ -k_f & 0 & k_f \\ 0 & \frac{1}{J_m} & 0 \end{pmatrix}$, $B = \begin{pmatrix} 0 \\ 0 \\ \frac{1}{J_m} \end{pmatrix}$, $C = \begin{pmatrix} 0 \\ 0 \\ 1 \end{pmatrix}$. To estimate

states x, the observer equation is

$$\begin{aligned}\dot{\hat{x}} &= A\hat{x} + Bu + B\hat{z} + L(y - \hat{y}) \\ \hat{y} &= C\hat{x}\end{aligned} \tag{18}$$

where $\hat{x}$, and $\hat{y}$ represent estimations of x, and y, respectively. $L = [l_1, l_2, l_3]^T$ is the design matrix which must be designed so that the observer is stable. $\hat{z} = -\hat{F}$ with $\hat{F}$ being the estimated lumped dynamics including frictions, which will be given by ESNs in the following Section.

Defining $\tilde{x} = x - \hat{x}$ estimation error dynamics are then given by

$$\dot{\tilde{x}} = \dot{x} - \dot{\hat{x}} = (A - LC)\tilde{x} + B\tilde{z} \tag{19}$$

where $\tilde{z} = z - \hat{z}$. The important question in observer synthesis is that choosing appropriate matrix $A - LC$ to ensure the stability of error dynamics (19). A stability condition of the matrix $A - LC$ is presented in [36].

3. Controller Design

The proposed controller is composed of a modified error constraint dynamic surface controller (ECDSC) and the friction compensator (FC). Choose state variable $x = [\ x_1 \quad x_2 \quad x_3\ ]^T = [\ \omega_l \quad m_s \quad \omega_m\ ]^T$. The system (1) can be written as

$$\frac{d}{dt}\begin{pmatrix} x_1 \\ x_2 \\ x_3 \end{pmatrix} = \begin{pmatrix} 0 & \frac{1}{J_l} & 0 \\ -k_f & 0 & k_f \\ 0 & \frac{1}{J_m} & 0 \end{pmatrix}\begin{pmatrix} x_1 \\ x_2 \\ x_3 \end{pmatrix} + \begin{pmatrix} 0 \\ 0 \\ \frac{1}{J_m} \end{pmatrix}(u - F) \tag{20}$$

Then the overall control u consists of a feedback control to retain tracking and an adaptive friction compensator, which will be designed in follow section.

3.1. Nonlinear High-Gain Tracking Differentiator

In [37], Guo proposed the nonlinear high-gain tracking differentiator (HGTD) to improve the performance of closed-loop control system. In this section, HGTD will be incorporated into the traditional DSC design procedure to obtain

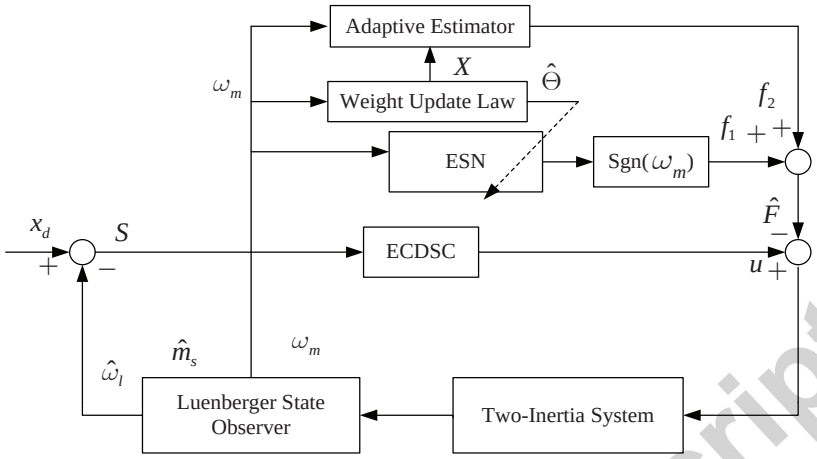

Figure 5: Closed-loop control diagram composed by two-inertia system, the ECDSC and FC.

the precise original intermediate control signals and the derivative signals. The form of HGTD is given as

$$\begin{cases} \dot{\vartheta}_{1i}(t) = \vartheta_{2i}(t) \\ \dot{\vartheta}_{2i}(t) = H^2 \left(-\rho_{1i}[\vartheta_1(t) - \bar{\chi}_i]^{\alpha} - \rho_{2i}[\vartheta_{2i}(t)/H]^{\beta}\right) \end{cases} \tag{21}$$

where ρ_i, α, β and H are positive design parameters. $\bar{\chi}_i$ represents the input signal of the HGTD, which is replaced by virtual intermediate control signal in the ECDSC design procedure.

Lemma 1 [37]: If the signal $\bar{\chi}_i$ satisfies, $sup_{t\in[0,\infty)}|\bar{\chi}_i^{(j)}| < \infty$ for $j = 1, 2$, then the first differentiator (22) is convergent for any initial value of (22) and $T > 0$, there exists $H > H_0 > 0$ and $t > T$, the following inequalities hold

$$\|\vartheta_{1i}(t) - \bar{\chi}_i\| \leq L_1(1/H)^{a/b}, |\vartheta_{2i}(t) - \dot{\bar{\chi}}_i| \leq L_2 \tag{22}$$

where L_1, L_2, a and b are constants.

The fast finite-time convergence makes it superior to linear filters in the control design and synthesis. When incorporated into the ECDSC design procedure, (21) can solve the explosion of complexity caused by differentiation of the intermediate control signals in conventional backstepping method.

3.2. Design ECDSC

In this section, a modified ECDSC with HGTD is developed for the nonlinear two-inertia system. The ECDSC is designed in the following steps.

Step 1: Define the first error surface as

$$S_1 = \hat{x}_1 - x_d. \tag{23}$$

from (16), we can obtain

$$z_1 = R_1 \left(\frac{S_1}{\lambda_1}\right) \tag{24}$$

The time derivative of z_1 is

$$\dot{z}_1 = r_1\big(\dot{S}_1 - \frac{\dot{\lambda}_1}{\lambda_1}S_1\big) = r_1\big(\hat{x}_2 - \dot{x}_d - \frac{\dot{\lambda}_1}{\lambda_1}S_1\big) \tag{25}$$

where $r_1 = (1/2\lambda_1)[1/(\rho_1 + \underline{\delta}_1) - 1/(\rho_1 - \bar{\delta}_1)]$, and $\rho_1 = S_1/\lambda_1$.

To avoid the problem of "explosion of complexity" in traditional backstepping design methods [38], we let x_d go through a high-gain tracking differentiator as

$$\begin{cases} \dot{\vartheta}_{1,1} = \vartheta_{2,1} \\ \dot{\vartheta}_{2,1} = H^2\big(- \rho_{1,1}[\vartheta_{1,1} - x_d]^{\alpha} - \rho_{2,1}[\vartheta_{2,1}/H]^{\beta}\big) \end{cases} \tag{26}$$

where $H, \rho_{1,1}, \rho_{2,1}, \alpha$, and β are the positive constants, $\vartheta_{1,1}$ is the filter signal of the desired trajectory of x_d. The time derivative of z_1 is

$$\dot{z}_1 = r_1\big(\hat{x}_2 - \vartheta_{2,1} - \frac{\dot{\lambda}_1}{\lambda_1}S_1\big) \tag{27}$$

By defining $S_2 = \hat{x}_2 - \bar{\chi}_1$ as the second error surface, one obtains

$$\hat{x}_2 = S_2 + \bar{\chi}_1. \tag{28}$$

The error transformation can be expressed as $S_2 = \lambda_2 R_2^{-1}(z_2)$, Substituting (27) into (28) yields

$$\dot{z}_1 = r_1\big(\lambda_2 R_2^{-1}(z_2) + \bar{\chi}_1 - \vartheta_{2,1} - S_1\frac{\dot{\lambda}_1}{\lambda_1}\big). \tag{29}$$

In order to make (29) negative, a virtual control $\bar{\chi}_1$ is defined as

$$\bar{\chi}_1 = -k_1 z_1 - \bar{\delta}_1 \frac{r_1 z_1 \lambda_2^2}{|r_1 z_1 \lambda_2| + \mu_1} + S_1\frac{\dot{\lambda}_1}{\lambda_1} + \vartheta_{2,1}. \tag{30}$$

where $k_1 > 0$, $\bar{\delta}_1 > 0$ and $\mu_1 > 0$ are the design parameters.

Step 2: In order to eliminate the explosion of complexity problem, we introduce a new state vector $\vartheta_2 = [\vartheta_{1,2}, \vartheta_{2,2}]^T$, and let $\bar{\chi}_1$ pass through a high-gain tracking differentiator as

$$\begin{cases} \dot{\vartheta}_{1,2} = \vartheta_{2,2} \\ \dot{\vartheta}_{2,2} = H^2\big(- \rho_{1,2}[\vartheta_{1,2} - \bar{\chi}_1]^{\alpha} - \rho_{2,2}[\vartheta_{2,2}/H]^{\beta}\big) \end{cases} \tag{31}$$

where $\rho_{1,2}$ and $\rho_{2,2}$ are the design parameters. The derivative of z_2 is given as

$$\dot{z}_2 = r_2\big(\dot{S}_2 - \frac{\dot{\lambda}_2}{\lambda_2}S_2\big) = r_2\big(\dot{\hat{x}}_2 - \dot{\bar{\chi}}_1 - \frac{\dot{\lambda}_2}{\lambda_2}S_2\big) \tag{32}$$

where $r_2 = (1/2\lambda_2)[1/(\rho_2 + \underline{\delta}_2) - 1/(\rho_2 - \bar{\delta}_2)]$, and $\rho_2 = S_2/\lambda_2$.

The derivative of (32) is

$$\dot{z}_2 = r_2\big[k_f(x_3 - \hat{x}_1) - \vartheta_{2,2} - \frac{\dot{\lambda}_2}{\lambda_2}S_2\big] \tag{33}$$

By defining $S_3 = x_3 - \bar{\chi}_2$ as the third error surface, one obtains

$$x_3 = S_3 + \bar{\chi}_2. \tag{34}$$

Substituting (34) into (33) yields

$$\dot{z}_2 = r_2\big[k_f(\lambda_3 R_3^{-1}(z_3) + \bar{\chi}_2 - \hat{x}_1) - \vartheta_{2,2} - \frac{\dot{\lambda}_2}{\lambda_2}S_2\big] \tag{35}$$

Choose the virtual control $\bar{\chi}_2$ as

$$\bar{\chi}_2 = \frac{1}{k_f}\big(- k_2 z_2 + \vartheta_{2,2} + \frac{\dot{\lambda}_2}{\lambda_2}S_2\big) + \hat{x}_1 - \bar{\delta}_2\frac{r_2 z_2 \lambda_3^2}{|r_2 z_2 \lambda_3| + \mu_2}. \tag{36}$$

where $k_2 > 0$, $\bar{\delta}_2 > 0$ and $\mu_2 > 0$ are the design parameters.

Step 3: In the final design step, the controller u will be obtained. The last error surface is defined as

$$S_3 = x_3 - \bar{\chi}_2. \tag{37}$$

The time derivative of z_3 is

$$\begin{aligned} \dot{z}_3 &= r_3\big(\dot{S}_3 - \frac{\dot{\lambda}_3}{\lambda_3}S_3\big) = r_3\big(x_3 - \dot{\bar{\chi}}_2 - \frac{\dot{\lambda}_3}{\lambda_3}S_3\big) \\ &= r_3\big(- \frac{1}{J_m}\hat{x}_2 + \frac{1}{J_m}u - \frac{1}{J_m}F - \dot{\bar{\chi}}_2 - \frac{\dot{\lambda}_3}{\lambda_3}S_3\big) \end{aligned} \tag{38}$$

where $r_3 = (1/2\lambda_3)[1/(\rho_3 + \underline{\delta}_3) - 1/(\rho_3 - \bar{\delta}_3)]$, and $\rho_3 = S_3/\lambda_3$.

Again, a new state vector $\vartheta_3 = [\vartheta_{1,3}, \vartheta_{2,3}]^T$ is introduced, and let $\bar{\chi}_2$ pass through a high-gain tracking differentiator as

$$\begin{cases} \dot{\vartheta}_{1,3} = \vartheta_{2,3} \\ \dot{\vartheta}_{2,3} = H^2\big(- \rho_{1,3}[\vartheta_{1,3} - \bar{\chi}_2]^\alpha - \rho_{2,3}[\vartheta_{2,3}/H]^\beta\big) \end{cases} \tag{39}$$

where $\rho_{1,3}$ and $\rho_{2,3}$ are the design parameters.

Then, the variable $\dot{z}_3$ can be rewritten as

$$\dot{z}_3 = r_3\big[\frac{1}{J_m}u - \frac{1}{J_m}\hat{x}_2 - \frac{1}{J_m}F - \vartheta_{2,3} - \frac{\dot{\lambda}_3}{\lambda_3}S_3\big] \tag{40}$$

Finally, the control signal u is chosen to be

$$u = J_m\big(- k_3 z_3 + \vartheta_{2,3} + \frac{\dot{\lambda}_3}{\lambda_3}S_3\big) + \hat{x}_2 + \hat{F} \tag{41}$$

where $k_3 > 0$ is the design parameter, and $\hat{F}$ is the estimated of unknown friction F, which will be given in the following subsection.

3.3. ESNs Friction Compensation Design

In the above control design, the controller u is obtained, where the F was merged. To obtain $\hat{F}$, the ESNs will be introduced to compensate it in this paper.

Defined $\epsilon = \zeta - \zeta_0$, the friction expression of the two-inertia system can be written as follows:

$$\begin{aligned} F &= \sigma_0\zeta + \sigma_1\dot{\zeta} + \sigma_2\omega_m + d \\ &= \sigma_2\dot{\theta}_m + \big[f_c + (f_s - f_c)e^{-(\omega_m/\dot{\upsilon}_s)^2}\big]sgn(\omega_m) \\ &+ \sigma_0\epsilon\big[1 - \frac{1}{f_c + (f_s - f_c)e^{-(\omega_m/\dot{\upsilon}_s)^2}}|\omega_m|\big] + d. \end{aligned} \tag{42}$$

The first part $\sigma_2\omega_m + [f_c + (f_s - f_c)e^{-(\omega_m/\dot{\upsilon}_s)^2}]sgn(\omega_m)$ is a static function of the velocity. The second part $\sigma_2\omega_m + [f_c + (f_s - f_c)e^{-(\omega_m/\dot{\upsilon}_s)^2}]sgn(\omega_m) + \sigma_0\epsilon\big[1 - \frac{1}{f_c+(f_s-f_c)e^{-(\omega_m/\dot{\upsilon}_s)^2}}|\omega_m|\big]$ is scaled by the error ϵ due to the dynamic perturbation in friction. Then

$$F \le \Delta_1|\omega_m| + \Delta_2 + \big[f_c + (f_s - f_c)e^{-(\omega_m/\dot{\upsilon}_s)^2}\big]sgn(\omega_m) \tag{43}$$

where ϵ is bounded since σ and σ_0 are bounded. Δ_1 and Δ_2 are positive constants. Let $f_1 = f_c + (f_s - f_c)e^{-(\omega_m/\dot{v}_s)^2}$, and $f_2 = \Delta_1|\omega_m| + \Delta_2$. Then (43) can be rewritten as

$$F \leq f_1 sgn(\omega_m) + f_2. \tag{44}$$

Since (44) is not a smooth function, it cannot be directly approximated via ESNs. However, f_1 is smooth function, which is compensated by ESNs as follows:

$$\hat{f}_1 = \hat{\Theta}^T X(x) \tag{45}$$

where $\hat{\Theta}$ is the estimation of Θ^*. Then, the updated learning algorithm is given as

$$\dot{\hat{\Theta}} = \Gamma_\Theta\big(r_3 z_3 X sgn(\omega_m) - \varrho_1 \hat{\Theta}\big) \tag{46}$$

where $\tilde{\Theta} = \hat{\Theta} - \Theta^*$ and Γ_Θ, $\varrho_1 > 0$.

Moreover, an adaptive estimator is employed to estimate f_2, and one can obtain

$$\hat{f}_2 = \hat{\Delta}_1|\omega_m| + \Delta_2 \tag{47}$$

where $\hat{\Delta}_1$ is the estimate of Δ_1. Then, the estimation algorithm is provided by

$$\dot{\hat{\Delta}}_1 = \Gamma_{\Delta_1}(r_3 z_3|\omega_m| - \varrho_2 \hat{\Delta}_1) \tag{48}$$

where Γ_{Δ_1} and ϱ_2 are positive constants.

From (45)-(48), one can obtain the friction compensation controller as

$$\hat{F} = \hat{f}_1 sgn(\omega_m) + \hat{f}_2. \tag{49}$$

Then, the controller u is given by

$$u = J_m\big(-k_3 z_3 + \vartheta_{2,3} + \frac{\dot{\lambda}_3}{\lambda_3} S_3\big) + \hat{x}_2 + \hat{f}_1 sgn(\omega_m) + \hat{f}_2 \tag{50}$$

4. Stability Analysis

In this section, the stability of closed-loop system is proved by Lyapunov stability theory.

Theorem 1: Consider the closed-loop system (1), for any bounded initial conditions, actual controller (50), the virtual controllers (30), (36), and friction compensation controller (49), adaptive laws (46) and (48) guarantee that all the signals in the resulting closed-loop are semiglobally uniformly ultimately bounded (SGUUB). Moreover, the tracking error and observer errors can be made arbitrarily small by choosing the design parameters.

Proof Consider Lyapunov function candidate as

$$V = \frac{1}{2}\sum_{i=1}^{3} z_i^2 + \frac{1}{2}\tilde{\Theta}^T\Gamma_{\Theta}^{-1}\tilde{\Theta} + \frac{1}{2}\Gamma_{\Delta_1}^{-1}\tilde{\Delta}_1^2. \tag{51}$$

Taking the time derivative of V, and Substituting (30), (36), (50), (46) and (48) into (51), it can be shown that

$$\begin{aligned}
\dot{V} &= \sum_{i=1}^{3} z_i\dot{z}_i + \tilde{\Theta}^T\Gamma_{\Theta}^{-1}\dot{\tilde{\Theta}} + \tilde{\Delta}_1\Gamma_{\Delta_1}^{-1}\dot{\tilde{\Delta}}_1 \\
&= r_1 z_1\big(\lambda_2 R_2^{-1}(z_2) + \bar{\chi}_1 - \vartheta_{2,1} - S_1\frac{\dot{\lambda}_1}{\lambda_1}\big) + r_2 z_2\big[k_f(\lambda_3 R_3^{-1}(z_3) + \bar{\chi}_2 - \hat{x}_1) - \vartheta_{2,2} \\
&- \frac{\dot{\lambda}_2}{\lambda_2}S_2\big] - r_3 z_3\big[\frac{1}{J_m}u - \frac{1}{J_m}\hat{x}_2 - \frac{1}{J_m}F - \vartheta_{2,3} - \frac{\dot{\lambda}_3}{\lambda_3}S_3\big] - \frac{1}{\Gamma_{\Theta}}\tilde{\Theta}^T\dot{\tilde{\Theta}} - \frac{1}{\Gamma_{\Delta_1}}\tilde{\Delta}_1^T\dot{\tilde{\Delta}}_1 \\
&= r_1 z_1\big(-k_1 z_1 + \lambda_2 R_2^{-1}(z_2) - \bar{\delta}_1\frac{r_1 z_1\lambda_2^2}{|r_1 z_1\lambda_2| + \mu_1}\big) + r_2 z_2\big(-k_2 z_2 + \lambda_3 R_3^{-1}(z_3) \\
&- \bar{\delta}_2\frac{r_2 z_2\lambda_3^2}{|r_2 z_2\lambda_3| + \mu_2}\big) + r_3 k_3 z_3^2 - \tilde{\Theta}^T\big(r_3 z_3 X sgn(\omega_m) - \frac{1}{\Gamma_{\Theta}}\dot{\hat{\Theta}}\big) - \tilde{\Delta}_1^T\big(r_3 z_3|\omega_m| - \frac{1}{\Gamma_{\Delta_1}}\dot{\hat{\Delta}}_1\big)
\end{aligned} \tag{52}$$

Using the Young's inequality, one has

$$\varrho_1\tilde{\Theta}^T\hat{\Theta} \le -\frac{\varrho_1}{2}\tilde{\Theta}^T\tilde{\Theta} + \frac{\varrho_1}{2}\Theta^2 \tag{53}$$

$$\varrho_2\tilde{\Delta}_1\hat{\Delta}_1 \le -\frac{\varrho_2}{2}\tilde{\Delta}_1^T\tilde{\Delta}_1 + \frac{\varrho_2}{2}\Delta_1^2. \tag{54}$$

Substituting (53) and (54) into (52) results in

$$\begin{aligned}
\dot{V} &\le -r_1 k_1 z_1^2 - r_2 k_2 z_2^2 - r_3 k_3 z_3^2 - \frac{\varrho_1}{2}\tilde{\Theta}^T\tilde{\Theta} - \frac{\varrho_2}{2}\tilde{\Delta}_1^T\tilde{\Delta}_1 + \frac{\varrho_1}{2}\Theta^2 + \frac{\varrho_2}{2}\Delta_1^2 \\
&\le -\pi\ V + \iota
\end{aligned} \tag{55}$$

where π and ι are positive constants, i.e.,

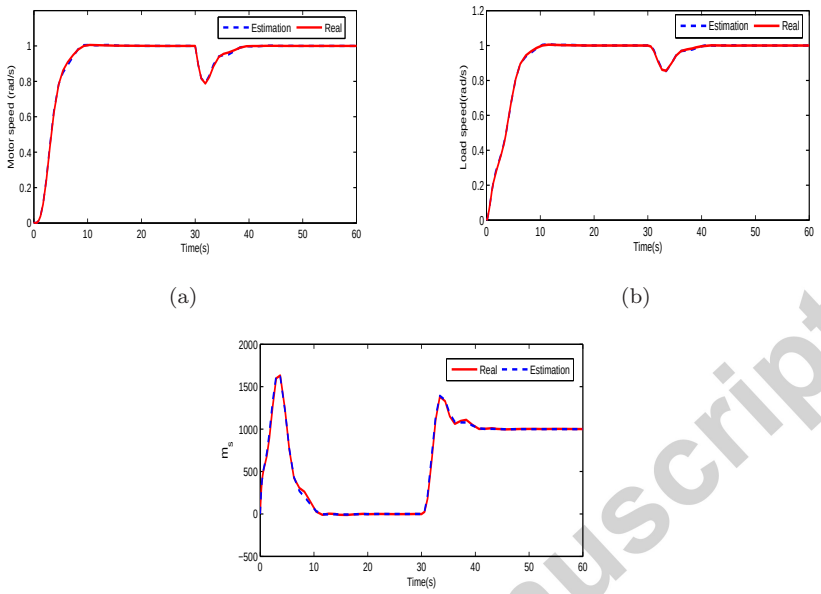

Figure 6: Transients of the real, estimated by Luenberger state observer and its estimation error: (a) motor speed, (b) load speed, and (c) torsional torques.

$\pi = min\{2r_1k_1, 2r_2k_3, 2r_3k_3\varrho_1, \varrho_2\}$, $\iota = \frac{\varrho_1}{2}\Theta^2 + \frac{\varrho_2}{2}\Delta_1^2$.

Solving this inequality yields

$$0 \leq V(t) \leq \left(V(0) - \frac{\iota}{\pi}\right) e^{-\pi t} + \frac{\iota}{\pi} \leq V(0)e^{-\pi t} + \frac{\iota}{\pi}. \tag{56}$$

From (55), $V(t)$ is eventually bounded by ι/π , which can be made arbitrarily small via designing controller parameters. Therefore, all the error signals are semiglobally, uniformly and ultimately bounded, and the $|S(t)| \leq \sqrt{2V(0)}e^{-\iota t} + \sqrt{2\iota/\pi}$. As $t \longrightarrow \infty$, $e^{-\pi t} \longrightarrow 0$, it follows that $|S(t)| \leq \sqrt{2\iota/\pi}$. Moreover, the bound $|S(t)| \leq \sqrt{2\iota/\pi}$ can be made as small as possible by choosing the design parameters. Therefore, the transient performance of the system is guaranteed with the prescribed performance bound for all $t \geq 0$. This completes the proof.

Remark 1: In the proposed control scheme, the initial condition $-\underline{\delta}\lambda(0) < e(0) < \overline{\delta}\lambda(0)$ should be guaranteed by designing the PPF parameters λ_0, $\underline{\delta}$ and $\overline{\delta}$, so that $z_i(0)$ is finite.

Remark 2: It is noted that many parameters are adjusted for applying the proposed control scheme for the nonlinear two-inertia system (1). From (55), we known that the bound of $|S(t)| \leq \sqrt{2\iota/\pi}$ depends on parameters ι and π. Increasing constant π and decreasing constant ι lead to small tracking error, i.e., increasing $k_i(i = 1, 2, 3)$ and decreasing $\mu_i(i = 1, 2)$. If μ_i is too small, it may not be sufficient to prevent the parameter estimates from the drifting. If k_i is large, the control energy is significant. Therefore, in practice, the design parameters should be chosen to trade off the transient and steady-state performance.

Remark 3: Compared with the traditional backstepping controller, the proposed ECDSC does not involve $\dot{\bar{\chi}}_i$, this will avoid the explosion of complexity caused by repeatedly differentiating $\bar{\chi}_i$, and can reduce the computational costs. In additional, the ECDSC is designed by introducing HGTD to replace the first-order filter in each recursive step, the transient convergence of filter performance on closed-loop stability can be improved though slightly increased computational cost should be used in comparison to first order filter. The prescribed performance function is integrated into controller design, which guarantees the tracking error within the prescribed region.

5. Simulation Results

In this section, the nonlinear frictions, parameters uncertainties and external disturbance are taken into consideration. The ECDSC with direct feedbacks from all the state variables is first tested for the nonlinear two-inertia system. The system model is constructed as Figure 1. In fact, the coefficients J_m, k_f, J_l are considered to be constant. The LG model is used to represent the friction dynamics. The system parameters are given as $J_m = 0.005kg \cdot m$, $J_l = 0.04kg \cdot m$, $k_f = 5$, the prescribed performance function parameters are chosen as $\lambda_0 = 1.2$, $\lambda_\infty = 0.1$, $c_i = 0.5$, and $\underline{\delta}_i = -1$, $\overline{\delta}_i = 1.5$. For the ESNs design, the number of neurons in the input and hidden layers are 2 and 13, respectively. The initial weights are zero. Now, ECDSC parameters are given as $\rho_{1,i} = \rho_{2,i} = 1(i = 1, 2, 3)$, $H = 100$, $\alpha = 1/2$, $\beta = 2/3$, $\mu_1 = \mu_2 = 0.1$,

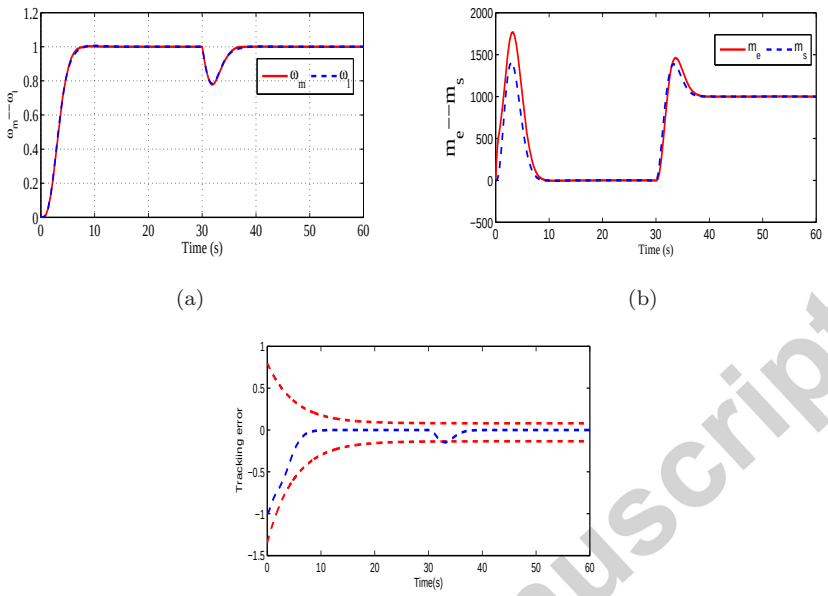

(a) (b)

(c)

Figure 7: Transients of the nonlinear two-inertia system by ECDSC : (a) motor speed and load speed (b) electromagnetic and torsional torques, and (c) tracking error.

$k_1 = 5, k_2 = 40, k_3 = 25$. As a comparison, an optimally tuned PID controller [1] is simulated for the nonlinear two-inertia system, the controller u is given as

$$u = \left(K_p + \frac{K_i}{s} + K_d s\right) e(t) \tag{57}$$

where $e(t)$ is the tracking error, and $K_p = 3.025$, $K_i = 0.015$ and $K_d = 0.0765$ represent the proportional, integral and derivative gains, respectively.

The simulation results are shown in Figures 6-10. The response curves of the real values and estimated values and their estimate errors are shown in Figure 6. From Figure 6, one can be observed that the estimation of the state variables can achieve the true values. In order to illustrate the effect of the parameters uncertainties and external disturbance on the transient performance of the control system, the step signal $d = 1$, is added to simulation at time $t = 0s$. The simulation results of proposed control scheme are shown in Figure 7. From Figure 7, one can see that the transient performance can be guaranteed

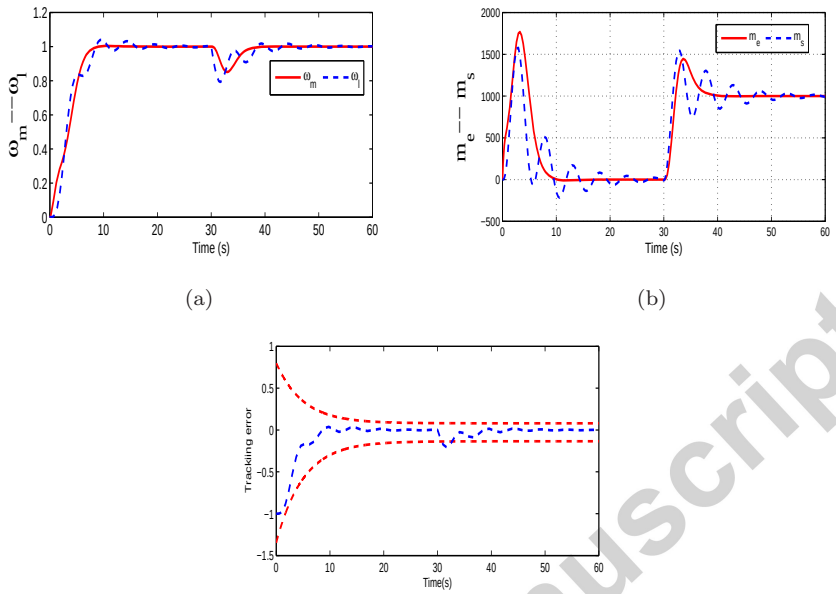

(a) (b)

(c)

Figure 8: Transients of the nonlinear two-inertia system by PID: (a) motor speed and load speed, and error, (b) electromagnetic and torsional torques, and (c) tracking error.

when there exist the the nonlinear friction, parameters uncertainties and external disturbance. The load-side speed can accurately track motor speed (Figure 7(a)), and there is no shaft torque oscillation (Figure 7(b)), which means that the torsional vibration is successfully damped. In addition, the tracking error is retained within prescribed performance bounds. As a comparison, the results of PID method are shown in Figure 8. It is clearly seen that the transient performance of load-side cannot be guaranteed, the load speed can not accurately track motor speed (Figure 8(a)), and the oscillation occurred (Figure 8(b)). Besides, the tracking error exceeds the prescribed performance boundary (Figure 8(c)).

Moreover, to study the effect of parameters uncertainties on the dynamic response of the nonlinear control system, the system parameters J_m and J_l subject to %5 uncertainties, i.e., $\Delta J_m = 0.05 J_m$ and $\Delta J_l = 0.05 J_l$, respectively. The simulation results are shown in Figure 9. As seen, although the speed and

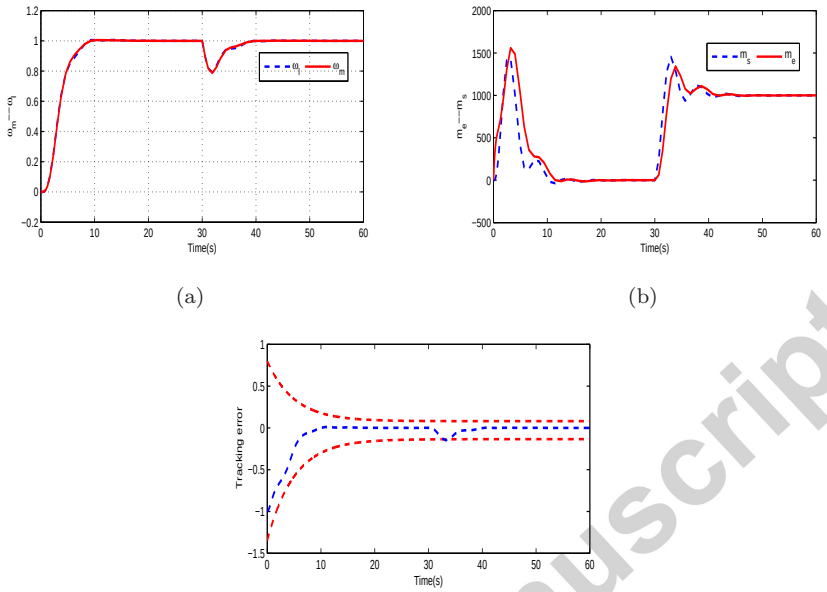

(a) (b)

(c)

Figure 9: Transients of the nonlinear two-inertia system by ECDSC (the system parameters J_m and J_l subject to %5 uncertainties): (a) motor speed and load speed, and error, (b) electromagnetic and torsional torques, and (c) tracking error.

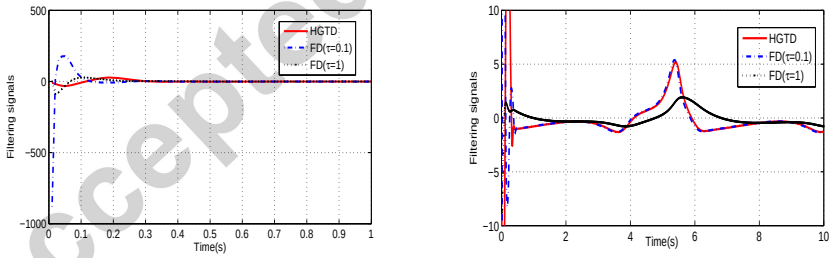

(a) (b)

Figure 10: (a) Transient performance of HGTD and FD, (b) Steady-state performance of HGTD and FD

toque indicate fairly sluggish response, the dynamic performance of the control system can be guaranteed, and the tracking error has also been remained within prescribed boundary. From Figure 7 and Figure 9, it is clearly seen that the proposed control scheme can guarantee the dynamic performance of the control

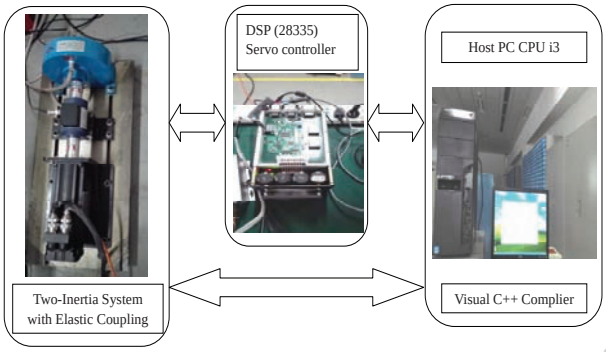

Figure 11: Diagram of the laboratory test rig

system when the parameters uncertainties exists in control system.

Figure 10 shows the filter effect of HGTD and first-order filter(FD). It can be found that both the transient and steady-state performance of HGTD are better than that of first-order filter. In particular, for the first-order filter with a large time constant ($\tau = 1$), the steady-state performance is the same as that of HGTD. However, the transient performance of first-order filter will deteriorate, as shown in Figure 9. Thus, one can conclude that the filter effect of HGTD is better than first-order filter.

6. Experimental results

6.1. Experimental setup

A realistic two-inertia system is used as the test-rig to validate the suggested control method. The configuration of the whole experimental setup is shown in Figure 11. The experimental setup is composed of the permanent-magnet synchronous motors connects to a load, PC with a 2.0GHz i5 CPU and 2G memory, and a digital signal processor (DSP, 28335). The control algorithms are written by Visual C++ program. The sampling time in the experiment setup is 0.1 ms. Nominal parameters of the drive system are presented in Table 1. The motor speed is measured by speed sensor in the test rig. However, the state variables such as torsional torque and load speed can not be measured,

Table 1: Parameters of the two-inertia system

Parameter	Value	Unit
Power	1.5	kW
Nominal motor voltage	230	V
Shaft length	40	cm
Nominal speed	3600	r/min
Motor inertia J_m	0.0062	$Kg \cdot m$
Load inertia J_l	0.004106	$Kg \cdot m$
Stiffness coefficient k_f	65	$N \cdot m$

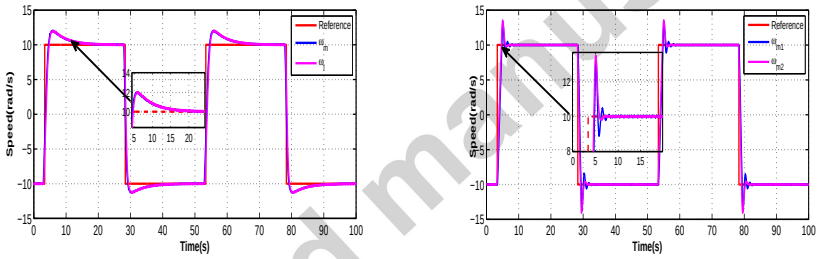

(a) (b)

Figure 12: Transients performance and tracking performance for square wave (a)ECDSC, (b)PID

the Luenberger state observer is employed to estimate the unmeasured state variables.

6.2. Controller design

The controller parameters are given as $\rho_{1,i} = \rho_{2,i} = 1(i = 1, 2, 3)$, $H = 100$, $\alpha = 1/2$, $\beta = 2/3$, $\mu_1 = \mu_2 = 0.1$, $k_1 = 2, k_2 = 10, k_3 = 15$. The prescribed performance function parameters are $\lambda_0 = 4$, $\lambda_\infty = 1$, $c_j = 3$, and $\underline{\delta}_j = 1.5$, $\overline{\delta}_j = 2$, $j = 1, 2$. The ESNs parameters are the same as simulation. The PID parameters are $K_p = 4$, $K_i = 0.25$ and $K_d = 0.03$.

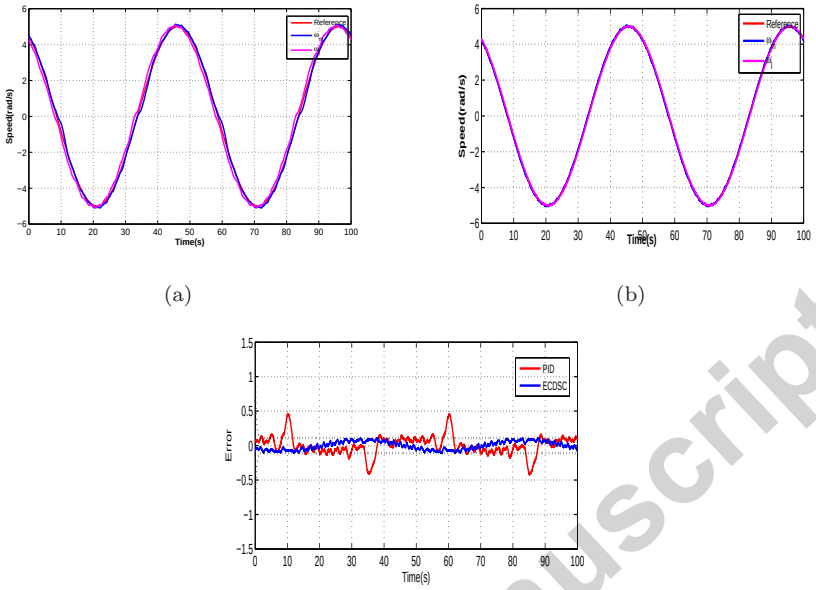

(a) (b)

(c)

Figure 13: Tracking performance and tracking performance for sinusoid wave (a)PID, (b)ECDSC, and (c)tracking error

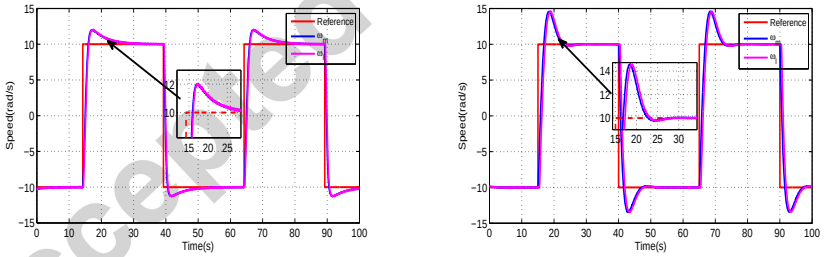

(a) (b)

Figure 14: Transients performance of the nonlinear two-inertia system for extra disturbance (a) ECDSC with FC ,and (b) ECDSC without FC

6.3. Experimental results

Extensive experiments have been carried out on the two-inertia system to show the effect of the proposed control scheme. First, the square-wave (Amplitude = 10) reference signal is adopted to illustrate the effect of the nonlinear

Table 2: Comparison for four indexes of difference signals.

	Square $A = 10$		$x_d = 5sin(0.4\pi t)$	
	PID	ECDSC	PID	ECDSC
IAE	23.3425	18.1953	9.7886	8.9597
ISDE	44.8311	37.8127	1.8276	0.9904
IAU	51.3472	38.1271	25.2047	23.3677
ISDU	171.0418	85.4938	8.7423	7.9858

friction, parameters uncertainties and external disturbance on transient response of the two-inertia system. The experiment results are shown in Figure 12. Figure 12(a) shows that the tracking performance and vibration suppression of the ECDSC is better than PID (Figure 12(b)), the overshoot is smaller than PID and there is no torsional vibration. To further show the effect of the parameters uncertainties and external disturbance on the dynamic performance of the two-inertia system, the sinusoid signal $x_d = 5\sin(0.4\pi t)$ is adopted as reference signal and the step signal $d = 1$ is adopted at time $t = 1s$ as a disturbance signal is added to experiment, and the experiment results are shown in Figure 13. One can see that, compared with the PID method, the tracking performance of proposed ECDSC is satisfactory, and the torsional vibration is damped. The tracking error is smaller than PID (Figure 13(c)), and the robustness of proposed control scheme is guaranteed when the external disturbance is added to experiment. To illustrate the effect of the friction compensation. Figure 14 shows the transients performance of the ECDSC with friction compensation and without friction compensation when the extra disturbance is added to experiment. From Figure 14, one can see that the proposed control scheme is effective to suppress the extra disturbance and guarantee dynamic response of the nonlinear system

To further show the efficacy and compare the control performance, four indices are adopted [39]; 1)integrated absolute error $IAE = \int |S_1(t)|dt$; 2)integrated square error $ISDE = \int (S_1(t) - S_0)^2 dt$, where S_0 is the mean value of

Table 3: Comparison for three indexes of difference signals.

	Square $A = 10$		$x_d = 5sin(0.4\pi t)$	
	PID	ECDSC	PID	ECDSC
M_e	3.8872	2.6507	0.5630	0.1407
μ	0.2334	0.1820	0.2594	0.0896
σ	0.0022	0.0018	0.002	0.0016

error; 3)integrated absolute control $IAU = \int |u(t)|dt$; and 4)integrated square control $ISDU = \int (u(t) - u_0)^2 dt$, where u_0 is the mean value of the control signal. The results are shown in Table 2. From Table 2, it is clearly shown that the proposed ECDSC performs better than PID control method for different reference signal. The four indices of proposed control scheme are smaller than PID control scheme.

Moreover, another three performance indexes are used to measure the quality of each control algorithm, i.e., maximal absolute value of the tracking errors $M_e = \max_{t=1,..,T}\{|S_1(t)|\}$, average tracking error $\mu = \frac{1}{T}\int |S_1(t)|dt$, and standard deviation of the tracking errors $\sigma = \sqrt{\frac{1}{T}\int [|S_1(t)| - \mu]^2 dt}$. The performance indexes are given in Table 3. From Table 3, one can clearly see that all performance indexes of the proposed control scheme are better than the PID control method for different input signals.

7. Conclusion

This paper proposes a vibration suppression control design method for elastically coupled two-inertia system based on ECDSC with friction compensation. The torsional vibrations of the two-inertia system are effectively suppressed using the control structure with recursive feedbacks from the load speed, torsional torque and motor speed. The unmeasured feedback signals are estimated by using a Luenberger state observer. The nonlinear friction is compensated by using the ESNs. The stability of the closed-loop system is ensured by Lyapunov

method and the tracking error is retained within the prescribed performance bounds. Comparative simulation and experiment results are obtained to illustrate the effectiveness of the proposed control scheme. In the future work, we will focus on extending the suggested control to two-inertia system with unknown parameters such as load inertia, elastic coefficients and motor inertia.

Acknowledgement

This work is supported by the National Natural Science Foundation of China (61433003, 61273150, 61573174, 61321002), the Research Fund for the Doctoral Program of Higher Education of China (20121101110029).

References

[1] G. Zhang, Speed control of two-inertia system by pi/pid control, Industrial Electronics, IEEE Transactions on 47 (3) (2000) 603–609.

[2] K. Szabat, T. Orlowska-Kowalska, Vibration suppression in a two-mass drive system using pi speed controller and additional feedbacks – comparative study, Industrial Electronics, IEEE Transactions on 54 (2) (2007) 1193–1206.

[3] T. O'Sullivan, C. Bingham, N. Schofield, High-performance control of dual-inertia servo-drive systems using low-cost integrated saw torque transducers, Industrial Electronics, IEEE Transactions on 53 (4) (2006) 1226–1237.

[4] K. Sugiura, Y. Hori, Vibration suppression in 2- and 3-mass system based on the feedback of imperfect derivative of the estimated torsional torque, Industrial Electronics, IEEE Transactions on 43 (1) (1996) 56–64.

[5] J. N. Yun, J. Su, Y. I. Kim, Y. C. Kim, Robust disturbance observer for two-inertia system, Industrial Electronics, IEEE Transactions on 60 (7) (2013) 2700–2710.

[6] K. Peter, I. Scholing, B. Orlik, Robust output-feedback h infin; control with a nonlinear observer for a two-mass system, Industry Applications, IEEE Transactions on 39 (3) (2003) 637–644.

[7] J.-K. Ji, S.-K. Sul, Kalman filter and lq based speed controller for torsional vibration suppression in a 2-mass motor drive system, Industrial Electronics, IEEE Transactions on 42 (6) (1995) 564–571.

[8] Y. Wei, J. Qiu, H. R. Karimi, M. Wang, A new design of filtering for continuous-time markovian jump systems with time-varying delay and partially accessible mode information, Signal Processing 93 (9) (2013) 2392 – 2407.

[9] Y. Wei, X. Peng, J. Qiu, S. Jia, filtering for two-dimensional continuous-time markovian jump systems with deficient transition descriptions, Neurocomputing 167 (2015) 406 – 417.

[10] S. Beineke, F. Schütte, H. Grotstollen, Comparison of methods for state estimation and on-line identification in speed and position control loops, in: Proc. of the Intern. Conf. European Power Electronics, 1997, pp. 3–364.

[11] K. Erenturk, Nonlinear two-mass system control with sliding-mode and optimised proportional-integral derivative controller combined with a grey estimator, Control Theory Applications, IET 2 (7) (2008) 635–642.

[12] T. Orlowska-Kowalska, K. Szabat, Neural-network application for mechanical variables estimation of a two-mass drive system, Industrial Electronics, IEEE Transactions on 54 (3) (2007) 1352–1364.

[13] T. Orlowska-Kowalska, M. Dybkowski, K. Szabat, Adaptive sliding-mode neuro-fuzzy control of the two-mass induction motor drive without mechanical sensors, Industrial Electronics, IEEE Transactions on 57 (2) (2010) 553–564.

[14] T. Orlowska-Kowalska, K. Szabat, Damping of torsional vibrations in two-mass system using adaptive sliding neuro-fuzzy approach, Industrial Informatics, IEEE Transactions on 4 (1) (2008) 47–57.

[15] K. Szabat, T. Tran-Van, M. Kaminski, A modified fuzzy luenberger observer for a two-mass drive system, Industrial Informatics, IEEE Transactions on 11 (2) (2015) 531–539.

[16] K. Itoh, M. Iwasaki, N. Matsui, Optimal design of robust vibration suppression controller using genetic algorithms, Industrial Electronics, IEEE Transactions on 51 (5) (2004) 947–953.

[17] M. Iwasaki, M. Miwa, N. Matsui, Ga-based evolutionary identification algorithm for unknown structured mechatronic systems, Industrial Electronics, IEEE Transactions on 52 (1) (2005) 300–305.

[18] D. Liu, T.-S. Chang, Y. Zhang, A constructive algorithm for feedforward neural networks with incremental training, Circuits and Systems I: Fundamental Theory and Applications, IEEE Transactions on 49 (12) (2002) 1876–1879.

[19] H. Patino, D. Liu, Neural network-based model reference adaptive control system, Systems, Man, and Cybernetics, Part B: Cybernetics, IEEE Transactions on 30 (1) (2000) 198–204.

[20] X. Ren, F. L. Lewis, J. Zhang, Neural network compensation control for mechanical systems with disturbances, Automatica 45 (5) (2009) 1221 – 1226.

[21] Z. Chen, S. S. Ge, Y. Zhang, Y. Li, Adaptive neural control of mimo nonlinear systems with a block-triangular pure-feedback control structure, Neural Networks and Learning Systems, IEEE Transactions on 25 (11) (2014) 2017–2029.

[22] T. Wang, H. Gao, J. Qiu, A combined adaptive neural network and nonlinear model predictive control for multirate networked industrial process

control, Neural Networks and Learning Systems, IEEE Transactions on PP (99) (2015) 1–1. doi:10.1109/TNNLS.2015.2411671.

[23] J. Qiu, S. Ding, H. Gao, S. Yin, Fuzzy-model-based reliable static output feedback h-infinity control of nonlinear hyperbolic pde systems, Fuzzy Systems, IEEE Transactions on PP (99) (2015) 1–1. doi:10.1109/TFUZZ.2015.2457934.

[24] H. Jaeger, The echo state approach to analysing and training recurrent neural networks-with an erratum note, Bonn, Germany: German National Research Center for Information Technology GMD Technical Report 148 (2001) 34.

[25] H. Jaeger, M. Lukosevicius, D. Popovici, U. Siewert, Optimization and applications of echo state networks with leaky- integrator neurons, Neural Networks 20 (3) (2007) 335 – 352, echo State Networks and Liquid State Machines.

[26] H. Jaeger, Adaptive nonlinear system identification with echo state networks, in: Advances in neural information processing systems, 2002, pp. 593–600.

[27] C. Bechlioulis, G. Rovithakis, Robust adaptive control of feedback linearizable mimo nonlinear systems with prescribed performance, Automatic Control, IEEE Transactions on 53 (9) (2008) 2090–2099.

[28] C. P. Bechlioulis, G. A. Rovithakis, Adaptive control with guaranteed transient and steady state tracking error bounds for strict feedback systems, Automatica 45 (2) (2009) 532 – 538.

[29] C. Bechlioulis, G. Rovithakis, Prescribed performance adaptive control for multi-input multi-output affine in the control nonlinear systems, Automatic Control, IEEE Transactions on 55 (5) (2010) 1220–1226.

[30] C. Bechlioulis, G. Rovithakis, A priori guaranteed evolution within the neural network approximation set and robustness expansion via prescribed

performance control, Neural Networks and Learning Systems, IEEE Transactions on 23 (4) (2012) 669–675.

[31] J. Na, Q. Chen, X. Ren, Y. Guo, Adaptive prescribed performance motion control of servo mechanisms with friction compensation, Industrial Electronics, IEEE Transactions on 61 (1) (2014) 486–494.

[32] Y. Huang, J. Na, X. Wu, X. Liu, Y. Guo, Adaptive control of nonlinear uncertain active suspension systems with prescribed performance, ISA transactions 54 (2015) 145–155.

[33] C. De Wit, H. Olsson, K. Astrom, P. Lischinsky, A new model for control of systems with friction, Automatic Control, IEEE Transactions on 40 (3) (1995) 419–425.

[34] W. Chen, K. Kong, M. Tomizuka, Dual-stage adaptive friction compensation for precise load side position tracking of indirect drive mechanisms, Control Systems Technology, IEEE Transactions on 23 (1) (2015) 164–175.

[35] G. Sun, D. Li, X. Ren, Modified neural dynamic surface approach to output feedback of mimo nonlinear systems, Neural Networks and Learning Systems, IEEE Transactions on 26 (2) (2015) 224–236.

[36] R. Rajamani, Observers for lipschitz nonlinear systems, Automatic Control, IEEE Transactions on 43 (3) (1998) 397–401.

[37] B.-Z. Guo, Z.-L. Zhao, Weak convergence of nonlinear high-gain tracking differentiator, Automatic Control, IEEE Transactions on 58 (4) (2013) 1074–1080.

[38] A.-M. Zou, Z.-G. Hou, M. Tan, Adaptive control of a class of nonlinear pure-feedback systems using fuzzy backstepping approach, Fuzzy Systems, IEEE Transactions on 16 (4) (2008) 886–897.

[39] J. Na, X. Ren, G. Herrmann, Z. Qiao, Adaptive neural dynamic surface control for servo systems with unknown dead-zone, Control Engineering Practice 19 (11) (2011) 1328 – 1343.